Biophysical Chemistry 335 (2026) 107647

Contents lists available at ScienceDirect

Biophysical Chemistry

journal homepage: www.elsevier.com/locate/biophyschem

How cholesterol modulates LL-37 function: A biophysical study in eukaryotic-like membrane systems

Juan M. Giraldo-Lorza [a], Saúl Antonio Hernández Martínez [b], Francisco J. Sierra-Valdez [b], Chad Leidy [c], Elizabeth Suesca [c], Marcela Manrique-Moreno [a,*]

[a] Chemistry Institute, Faculty of Exact and Natural Sciences, University of Antioquia, A.A. 1226, Medellin, Colombia
[b] Escuela de Ingeniería y Ciencias, Tecnológico de Monterrey, 64700 Monterrey, NL, Mexico
[c] Biophysics Group, Physics Deparment, Universidad de los Andes, 111711 Bogotá, Cundinamarca, Colombia

ARTICLE INFO

Keywords:
Eukaryotic membran
Human cathelicidin
LL-37
Membrane-peptide interactions

ABSTRACT

The limited selectivity of antimicrobial peptides (AMPs) can lead to unintended damage to healthy eukaryotic cells, a process strongly influenced by membrane physicochemical properties. Cholesterol (CHO) is a key regulator of lipid packing, membrane order, and bilayer mechanical stability; however, its role in modulating AMP–membrane interactions remain incompletely understood. Here, we examine how CHO alters peptide–membrane interactions at the molecular level using eukaryotic membrane models composed of phosphatidylcholine, sphingomyelin, and increasing CHO fractions.

Fourier-transform infrared spectroscopy (FT-IR), differential scanning calorimetry (DSC), isothermal titration calorimetry (ITC), and fluorescence spectroscopy were employed to probe both structural and thermodynamic changes upon interaction with the human cathelicidin LL-37. FT-IR and DSC revealed that LL-37 preferentially perturbs sphingomyelin-enriched membranes, inducing shifts in phase transition temperatures and signatures of domain segregation. These perturbations were pronounced in the absence of CHO and remained detectable up to 10 mol% CHO, but were markedly attenuated at 20 mol% CHO. ITC measurements confirmed a higher binding affinity of LL-37 for sphingomyelin-rich regions, whereas fluorescence permeabilization assays demonstrated a progressive increase in membrane resistance to peptide-induced disruption with increasing CHO content.

Collectively, these results suggest that LL-37 preferentially partitions into cholesterol-poor membrane domains, destabilizing their structure. In contrast, cholesterol incorporation stabilizes the surface of cholesterol-rich domain without necessarily promoting peptide anchoring within the bilayer. This study provides mechanistic insights into AMP cytotoxicity toward eukaryotic membranes and underscores cholesterol's protective role offering guidance for designing peptides with enhanced therapeutic selectivity.

1. Introduction

Cathelicidins are a family of mammalian antimicrobial peptides (AMPs) first discovered in 1995 [1]. They have gained immense interest in the past few years due to their properties of both innate and adaptive immune responses such as regulation of inflammation/chemotaxis, antimicrobial activity, antivirus, antifungal and antituberculosis [2–4]. More recently, evidence indicates that cathelicidins have more extensive roles in host defense, whereas dysregulated expressions of them lead to the onset and perpetuation of diseases [5,6]. Host defense peptides characteristically contain large sequences of basic amino acids, which are conserved in many cathelicidins [7]. Most of the cathelicidins

Abbreviations: AMPs, antimicrobial peptides; POPC, 1-palmitoyl-2-oleoyl-sn-glycerol-3-phosphocholine; DPPC, 1,2-dipalmitoyl-sn-glycero-3-phosphocholine; Egg-SM, Egg sphingomyelin; CHO, cholesterol; HEPES, N-2-hydroxyethylpiperazine-N′-2-ethanesulfonic acid; SLBs, supported lipid bilayers; LUVs, large unilamellar vesicles; MLVs, multilamellar vesicles; FT-IR, Fourier–transform infrared spectroscopy; ATR, attenuated total reflectance; DSC, differential scanning calorimetry; ITC, isothermal titration calorimetry; T_m, main transition temperature; ΔT_n, change of temperature in phase transition, where n is the number of peaks; $\upsilon_s CH_2$, methylene symmetric stretching; ΔH, change in enthalpy; ΔS, change un entropy; C_p, calorific capacity; Δ(ΔH), relative change in calorimetric enthalpy; ΔH_{Total}, total enthalpy change of phase transition; L_β, gel phase; L_α, liquid-crystalline phase or liquid disordered phase; L_o, liquid ordered phase.

* Corresponding author at: University of Antioquia, A.A. 1226, Calle 67 # 53-108 Office 2-235, Laboratory 1-314, Medellin, Colombia.
E-mail addresses: juan.giraldo77@udea.edu.co (J.M. Giraldo-Lorza), hernandez.saul@tec.mx (S.A. Hernández Martínez), f.sierra@tec.mx (F.J. Sierra-Valdez), cleidy@uniandes.edu.co (C. Leidy), e.suesca87@uniandes.edu.co (E. Suesca), marcela.manrique@udea.edu.co (M. Manrique-Moreno).

https://doi.org/10.1016/j.bpc.2026.107647
Received 19 January 2026; Received in revised form 16 April 2026; Accepted 6 May 2026
Available online 10 May 2026

characterized to date also exhibit immunomodulatory effects, some of them with host-beneficial properties [8]. It is indeed possible to state that from an evolutionary point of view, the cathelicidin family of molecules appears in the mammalian animal group as an important part of the innate immune defense, providing a sort of interface that connects the innate host defense with T-cell immune responses [6,8].

LL-37 (human cathelicidin, and a 37 amino acid peptide) is a multifunctional antimicrobial peptide with both antimicrobial and immunomodulatory properties. This peptide is expressed in neutrophils, skin, lung, intestine and other epithelia, where it contributes to the body's first line defense against infectious agents. LL-37 modulates inflammation by chemotaxis of neutrophils, monocytes, and T-cells, promoting wound healing and suppressing pro-inflammatory responses [9–11]. LL-37 also exerts anti-inflammatory effects through the inhibition of production of pro-inflammatory cytokines like IL-6, TNF-α and IL-1β [12]. However, LL-37 exhibits a high degree of cytotoxicity in both neutrophils and various epithelial and immune system-derived cells at concentrations not far above those occurring in inflamed tissues. Under physiological conditions, LL-37 accumulates in the sputum of bronchial epithelial cells where it can directly damage the function of the cilia lining the respiratory airways [13]. The mechanism by which LL-37 exert its antimicrobial activity has been primarily described based on electrostatic attraction to bacterial lipid membranes, insertion into the bilayer, and disruption via carpet- or toroidal pore-like mechanisms, leading to permeabilization and cell death [14].

Cholesterol (CHO) is the predominant sterol in eukaryotic membranes, comprising 10–50% of total lipids depending on cell type [15]. The biophysical and biochemical characteristics of membranes are strongly influenced by their lipid composition and organization [16]. In the CHO molecule, the hydroxyl group positions close to the hydrophilic/hydrophobic interface of the bilayer, with the ring structure extending into the acyl chain region and positioning itself parallel to the acyl chains, resulting in a reduction in rotational conformations of the chains. Acyl chain alignment induces an increase in bilayer thickness in regions enriched in CHO. The unique structure of CHO makes it especially important in modulating key membrane features such as lipid packing, fluidity, lateral organization, and bilayer curvature [17]. A molecule that can alter the physicochemical properties of the membrane also has the potential to influence the activity of membrane-active agents, such as AMPs [18].

This study investigated the effect of CHO on the membrane-disruptive effect of the human cathelicidin LL-37 with POPC:SM and POPC:SM:CHO membrane models through biophysical techniques. Because CHO markedly influences the activity of membrane-active peptides by strengthening lipid packing, inhibiting bilayer disruption, and hindering peptide interaction or insertion, CHO inclusion provides critical insight into peptide–membrane interactions under more physiologically relevant conditions [19–21]. In the previous work of our group we discussed the current interest in understanding how CHO can affect the interaction between AMPs and lipid membranes and how this can be used in the design of new peptides that act as antimicrobial agents without causing harm to human cells [18]. Synthetic lipid systems were built based on the representative phospholipids that constitute a eukaryotic membrane and analyzed by infrared spectroscopy (FT-IR), differential scanning calorimetry (DSC), isothermal titration calorimetry (ITC), and fluorescence spectroscopy. The outcomes offer valuable insights into how the lipid profile affects membrane-peptide interactions and help to understand how CHO is a key part of eukaryotic cell protection.

2. Material and methods

2.1. Reagents

1-palmitoyl-2-oleoyl-sn-glycerol-3-phosphocholine (POPC, Lot 160–181PC-204-100MG), 1,2-dipalmitoyl-sn-glycero-3-phosphocholine (DPPC, Lot 160PC-318), egg sphingomyelin (Egg SM, Lot 860061P-1G-A-116), and cholesterol (CHO, Lot 700000P) were purchased from Avanti Polar Lipids (Alabaster, AL, USA). The length of the acyl chains was selected for being the most abundant in the eukaryotic cells [22,23]. The N-2-hydroxyethylpiperazine-N′-2-ethanesulfonic acid (HEPES) was from Sigma-Aldrich (St. Louis, MO, USA). All other reagents of analytical grade were from Sigma-Aldrich.

LL-37 peptide (LLGDFFRKSKEKIGKEFKRIVQRIKDFLRNLVPRTES, Lot. U1440EE070–11/PE1324) was purchased from GenScript (Piscataway Township, NJ, USA) and synthesized according to the sequence by solid-phase method. The purity of the peptide was determined to be higher than 95% by analytical HPLC, TFA removal was performed, and the molecular weight was confirmed with MALDI-TOF mass spectrometry.

2.2. Fourier-transform infrared spectroscopy

Stock solutions (20 mM) of the individual lipids DPPC, SM, as well as multi-component lipid systems (POPC:SM at 50:50 mol%, and POPC:SM:CHO at 45:45:10, 40:40:20 mol%) were prepared in chloroform and stored at −20 °C. Because the FTIR equipment operates reliably between 5 and 100 °C, DPPC was selected instead of POPC for phase transition measurements, as its main melting transition occurs within this accessible temperature range. Lipid transition measurements were performed using a BioATR II cell coupled to a Tensor II spectrometer (Bruker Optics, Ettlingen, Germany) equipped with Mercury Cadmium Tellurium (MCT) detector. Spectra were acquired at a resolution lower than 0.4 cm^{-1}, and 120 scans per measured temperature. Temperature control was maintained with a Huber Ministat 125 circulating water bath (Huber, Offenburg, Germany), with an accuracy ±0.01 °C. For the phase transition measurements, 20 μL of buffer 20 mM HEPES (pH 7.4) was added to the silicon crystal of the ATR cell to record the background in a programmed temperature ramp range from 30 to 52 °C for DPPC, 25 to 47 °C for SM, and 5 to 55 °C for the multi-component lipid systems. The heating rate in all the experiments was 1 °C/min and equilibration time of 120 s between each measurement. After recording the background, the supported lipid bilayers (SLBs) were prepared in situ by adding 20 μL of the 20 mM lipid stock solution on the crystal, the solvent was evaporated, and the lipid multilayer film was hydrated using 20 μL of the same buffer at a temperature above the T_m for 10 min for all lipid systems; then, the samples were analyzed under the same temperature range set as the background. During hydration, the LL-37 peptide was added in the same buffer at different concentrations (1 to 10 mol%).

Spectral data processing was performed using the OPUS 3D software 8.4.4 version (Bruker Optics, Ettlingen, Germany), background subtraction was applied automatically. Phase transition temperatures were followed by the vibration of methylene groups (2970 to 2820 cm^{-1}); for that, the frequency range of the symmetric extension (2850 to 2853 cm^{-1}) was cut from the spectra with subsequent baseline correction using the 20% sensitivity rubber band method. The maximum wavenumber for the symmetric extension of each temperature was obtained using the peak picking tool of the OPUS software. Finally, the data were plotted as a wavenumber as a function of temperature, and to determine T_m, the experimental sigmoidal curve was fitted into a Boltzmann function with a Levenberg–Marquardt iteration algorithm to calculate the inflection point of the curve using Origin Pro 8.0 software (OriginLab Corporation, Northampton, MA, USA) [24]. Three independent experiments were performed to check the repeatability.

2.3. Liposomal preparation

Stock solutions of the pure lipids and the multi-component lipid systems (POPC:SM at 50:50 mol%, and POPC:SM:CHO at 45:45:10, 40:40:20 mol%) were dissolved in chloroform and mixed into an airtight amber borosilicate vial to be evaporated (55 °C and 550 rpm) under a nitrogen stream for 40 min using the heat and magnetic stirring features

of TA systems degasification station (TA systems, Rochester, USA). Dried lipid film was hydrated using a filtered buffer (20 mM HEPES, pH 7.4) prepared with deionized water (Milli-Q, 18.2 MΩ cm) to reach a final concentration of 1 mM. The hydrated sample was incubated during 45 min at 55 °C and 650 rpm to produce multilamellar vesicles (MLVs).

2.4. Isothermal titration calorimetry (ITC)

To investigate peptide binding to lipid systems, ITC experiments were conducted using an Affinity ITC Low Volume (TA Instruments, New Castle, DE, USA). MLVs sample was loaded into the calorimetric cell (350 μl), while peptide solution (1.5 mM) prepared in the same buffer was placed in the injection syringe. All samples were thoroughly degassed prior to loading. Following thermal equilibration, programmed to titrate 10 injections of 2.5 μL (300 s interval and 125 rpm). Heats of dilution for peptides in the buffer were subtracted from the respective experiment. The total heat released or absorbed during each experiment was calculated by integrating the area under each peak and then plotted as a function of the [peptide]:[lipid] molar ratio. Thermogram analysis was conducted through the NanoAnalyze software (v4.0.2.0, TA Instruments, New Castle, USA). All titration experiments were performed at 37 °C and were done by duplicate.

2.5. Differential scanning calorimetry (DSC)

After each duplicate of ITC experiment samples were collected and transferred to the DSC cell (700 μl), previously equilibrated at 40 °C. DSC measurements were performed using the Nano DSC Series III platinum capillary cell system (TA Instruments, New Castle, DE, USA). The reference cell was loaded with the same buffer solution. The cells were pressurized at 3 atm and equilibrated for 10 min at the starting temperature. All samples were analyzed by cooling scans performed at 1 °C per minute from −10 to 60 °C. For data processing, the reference scan was subtracted from the sample scan. Each data set was analyzed, and the values of transition temperature (T_m) enthalpy (ΔH) and entropy (ΔS) were calculated using the NanoAnalyze software 3.12.0 version (TA Instruments, New Castle, DE, USA). At least three independent experiments were performed. The experimental data was plotted using Origin Pro 8.0 software (OriginLab Corporation, Northampton, MA, USA).

2.6. Fluorescence spectroscopy

Three lipid systems: POPC:SM (50:50 mol%), POPC:SM:CHO (45:45:10 mol%) and POPC:SM:CHO (40:40:20 mol%) were prepared for the calcein leakage experiments. An appropriate amount of the lipids was dissolved using chloroform in glass test tubes to reach a concentration of 10 mM. The solvent was evaporated under a stream of nitrogen, and the samples were then kept under vacuum for at least 12 h to ensure complete solvent removal. The lipid films were hydrated and resuspended in a buffer (20 mM HEPES, 125 mM NaCl at pH 7.4) containing 50 mM calcein (400 mOsm). Test tubes were vortexed for 5 min to obtain MLVs. The calcein buffer was prepared as follows: 778.2 mg of calcein was dissolved in 5 mL of 1 M NaOH. After the calcein was fully dissolved, 2.5 mL of 10 × HEPES solution (100 mM HEPES) was added together with 5 mL of MilliQ water (Millipore, Bedford, MA, USA). Volume was completed dropwise with HCl in order to reach pH 7.4. An appropriate amount of NaCl solution was then added to reach a concentration of 400 mOsM. Finally, MilliQ water was then added to bring the calcein buffer to a final volume of 25 mL and a final calcein concentration of 50 mM. The sample was warmed to 60 °C for 5 min and vortexed for 1 min, this process was repeated five times.

Large Unilamellar Vesicles (LUVs) were obtained by extruding the suspension 21 times through two polycarbonate filters of 100 nm pore size, with the use of a mini extruder from Avanti Polar Lipids (Alabaster, AL, USA). The dye-containing vesicles were separated from non-entrapped calcein using a size exclusion chromatographic column Sephadex G50 (fine, 10 mm × 250 mm) eluted with HEPES buffer that did not contain calcein (calcein–LUVs). The collected samples were always kept warm before measurements were conducted. The fluorometer cuvette with buffer was always stabilized to a final temperature of 37 °C before adding the vesicles. Calcein leakage caused by loss of membrane integrity was induced by varying the concentration of peptide in the sample or, in the case of the osmotic stress experiments in the absence of peptides, by varying the ratio dH_2O/buffer in the cuvette. The complete release of calcein was achieved through the addition of 1% volume Triton-X. At least three independent experiments were performed to ensure repeatability. The apparent percentage of calcein release (normalized membrane leakage), was calculated according to the eq. (1):

$$L_T = \frac{F - F_0}{F_{100} - F_0} \times 100 \quad (1)$$

3. Results

3.1. Phase transitions measurements by FT-IR spectroscopy

Infrared spectroscopy experiments were conducted to investigate the interaction between LL-37 and three multicomponent lipid model systems: POPC:SM (50:50), POPC:SM:CHO (45:45:10), and POPC:SM:CHO (40:40:20). Using Attenuated Total Reflectance (ATR) mode, changes in the packing of the lipid bilayer were monitored by tracking the methylene symmetric stretching (υ_sCH_2) vibrational mode as a function of temperature. This vibrational feature serves as a sensitive indicator of lipid order and membrane packing [25,26]. Shifts in the peak wavenumber of the υ_sCH_2 band, originating from the hydrocarbon core of the bilayer, were analyzed in response to variations in temperature and LL-37 concentration. The results of the incubation of peptides with the three lipid models are presented in Fig. 1. The gel (L_β) to liquid-crystalline (L_α) phase transition of the POPC:SM (50:50) mixture exhibited a cooperative melting behavior, with the inflection point indicating the phase transition temperature of the main melting event (29.50 °C). At lower temperatures, corresponding to the lamellar gel phase, the υ_sCH_2 band appears near 2850 cm^{-1}. As the temperature increases and the membrane transitions to the liquid-crystalline phase, this band shifts toward approximately 2853 cm^{-1} (Fig. 1A). The incubation of the supported lipid bilayers with LL-37 induces a strong fluidization effect on the POPC:SM model system. Increasing concentrations of the AMP results in strong changes in the lipid packing in the gel phase and liquid-crystalline phase temperature regimes, as evidenced by the upward shift in the υ_sCH_2 band (Fig. 1A). This was accompanied by a shift of the T_m to lower temperatures in a concentration-dependent manner. At the lowest concentration evaluated (0.1 mol%) a reduction of 2.74 °C was observed, and at the highest concentration evaluated of the peptide (10 mol%), the change in the T_m was 7.8 °C (Table 1).

The incorporation of 10 and 20 mol% CHO into the POPC:SM model membrane decreases the cooperativity of the main melting transition and, as expected, results in a lower T_m for both lipid systems (Table 1). This corresponds to the formation of SM/CHO-enriched liquid-ordered phase domains (L_o) [27–29], characterized by ordered acyl chains with high lateral mobility [30]. Results of the incubation of LL-37 with the two lipid model systems containing CHO showed that increasing concentrations of CHO reduces the fluidizing activity of LL-37. At higher concentrations of CHO, the destabilizing effect of the peptide is further lowered (Fig. 1B-C). This effect can be observed when at fixed temperature the wavenumbers of the same peptide concentrations are compared for the lipid systems containing 10 and 20 mol% of CHO (Fig. 2). At 10 mol% CHO, the membrane is in an intermediate regime where cholesterol disrupts gel–liquid phase coexistence but does not yet establish a fully ordered liquid-ordered phase. In this state, packing

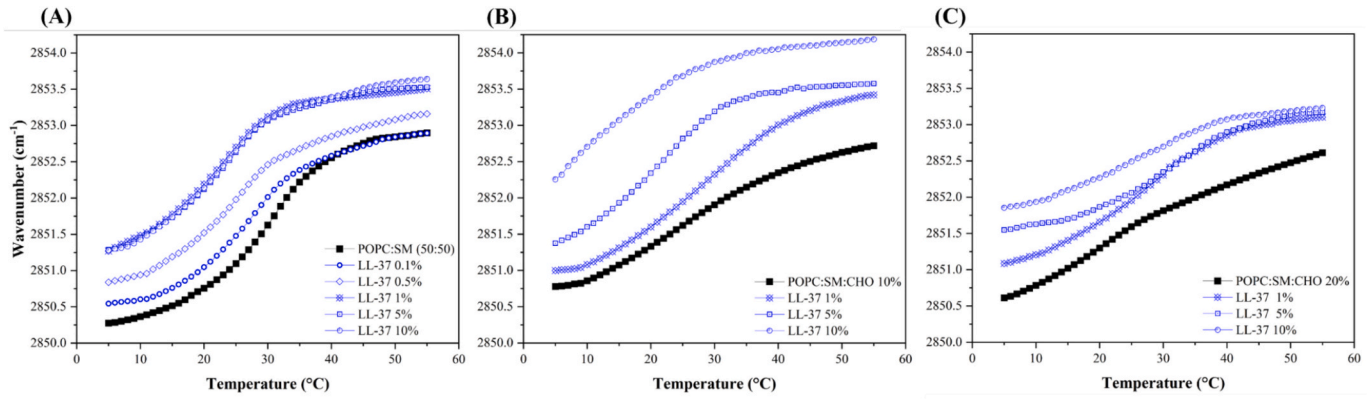

Fig. 1. Peak position of the symmetric stretching vibration band of the methylene groups as a function of temperature: Effect of different LL-37concentrations on **(A)** POPC:SM (50:50), **(B)** POPC:SM:CHO (45:45:10), and **(C)** POPC:SM:CHO (40:40:20) supported lipid bilayers in HEPES buffer 20 mM. The results represent three independent experiments.

Table 1
Phase transition temperatures (T_m) of the synthetic lipid systems in the presence of several concentrations of LL-37, as determined by FT-IR. Standard deviations are ≤0.1 °C.

Lipid System	T_m (°C)					
	LL-37 (mol%)					
	0	0.1	0.5	1	5	10
POPC:SM	29.5	26.8	24.1	21.2	21.9	21.7
POPC:SM:CHO 10%	25.3	–	–	27.7	20.4	7.8
POPC:SM:CHO 20%	17.7	–	–	26.2	30.5	25.1
DPPC	40.7	–	–	40.8	39.9	39.1
SM	38.6	–	–	37.6	37.5	35.2

means not determined.

defects and lateral heterogeneity are maximized, which can enhance peptide insertion. LL-37, being amphipathic and membrane-active, likely exploits these defects, leading to greater perturbation compared with POPC:SM without CHO. In contrast, at 20 mol% CHO, the membrane more clearly adopts a liquid-ordered phase, characterized by tighter lipid packing and reduced free volume. This limits peptide insertion and penetration, explaining why the increase in wavenumber (i.e., disorder/fluidization) is smaller despite higher peptide concentration. For POPC:SM without CHO, the bilayer lacks cholesterol-induced ordering but also lacks the defect structures seen at intermediate CHO levels. As a result, LL-37 interaction produces a moderate, more uniform perturbation, rather than the enhanced effect seen at 10% CHO.

With the aim of identifying if the membrane-disrupting activity of the peptide is specific to the phospholipids constituting the lipid models, separate thermotropic measurements by FT-IR were conducted with LL-37 and the pure phosphatidylcholine or sphingomyelin components of the mixture. The results of these experiments are summarized in Fig. 3. The SLBs of DPPC in HEPES showed a T_m of 40.7 °C, this result is in accordance with previous publications [31,32]. Incubation with LL-37 induced a fluidization effect in the gel and liquid-crystalline phase temperature regimes. In addition, the phase transition temperature is observed to decrease in a concentration-dependent manner.

In comparison, the sphingomyelin phase transition, in the absence of peptide, is characterized by a broad gel to liquid-crystalline transition centered at 38.6 °C, that is in accordance with previous reports in the literature [33,34]. At lower peptide concentrations (1–5 mol%), only a slight effect on the phase transition temperature is observed, while at 10 mol% the cooperativity of the transition is significantly broadened. The

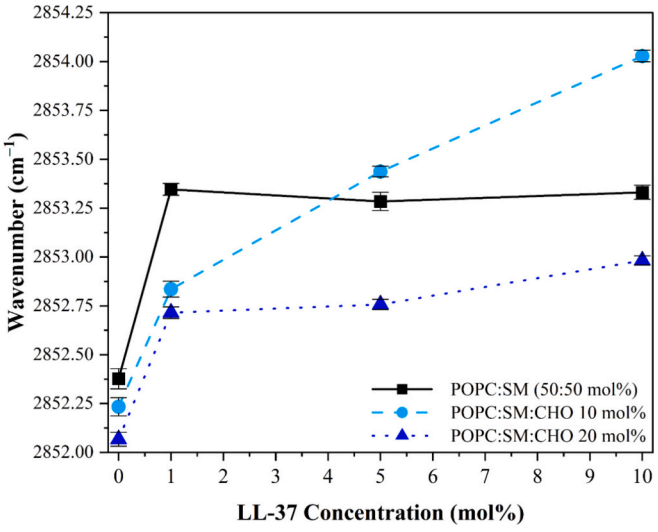

Fig. 2. Effect of LL-37 concentration on the symmetric CH_2 stretching vibration at 37 °C of POPC:SM (■, solid line), POPC:SM:CHO 10 mol% (●, dashed line), and POPC:SM:CHO 20 mol% (▲, dotted line) bilayers. Data are presented as mean ± SD of at least three independent measurements.

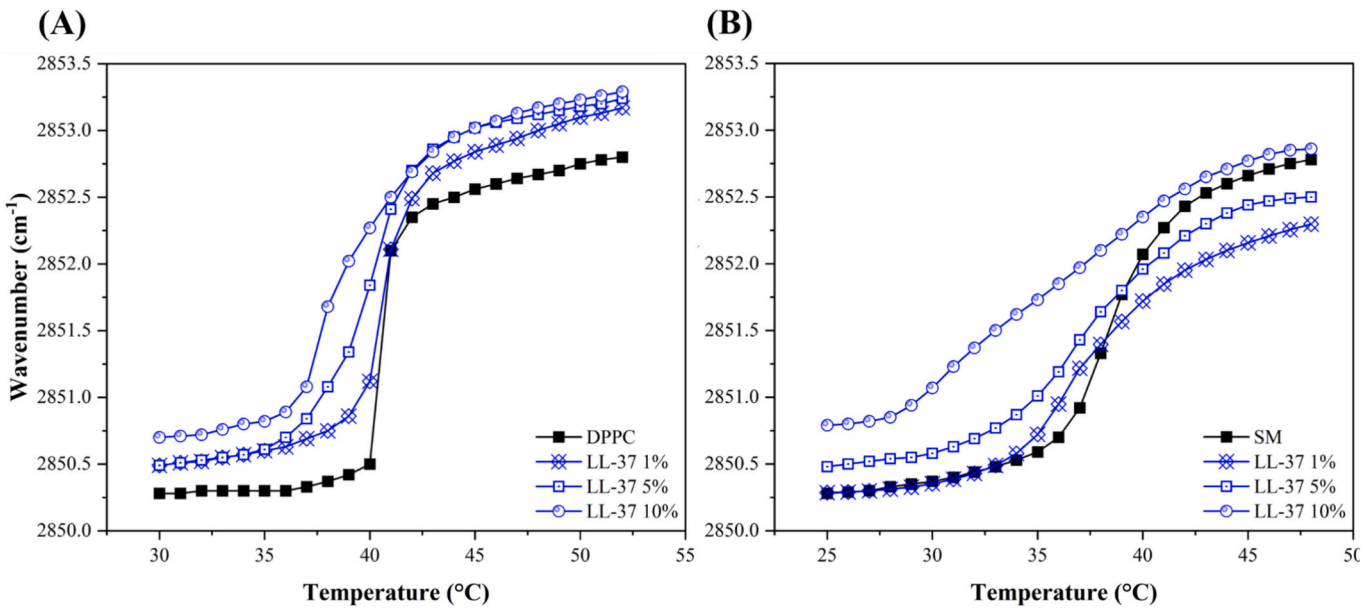

Fig. 3. Peak position of the symmetric stretching vibration band of the methylene groups as a function of temperature: Effect of different LL-37 concentrations on **(A)** DPPC and **(B)** SM supported lipid bilayers in HEPES buffer 20 mM. The results represent three independent experiments.

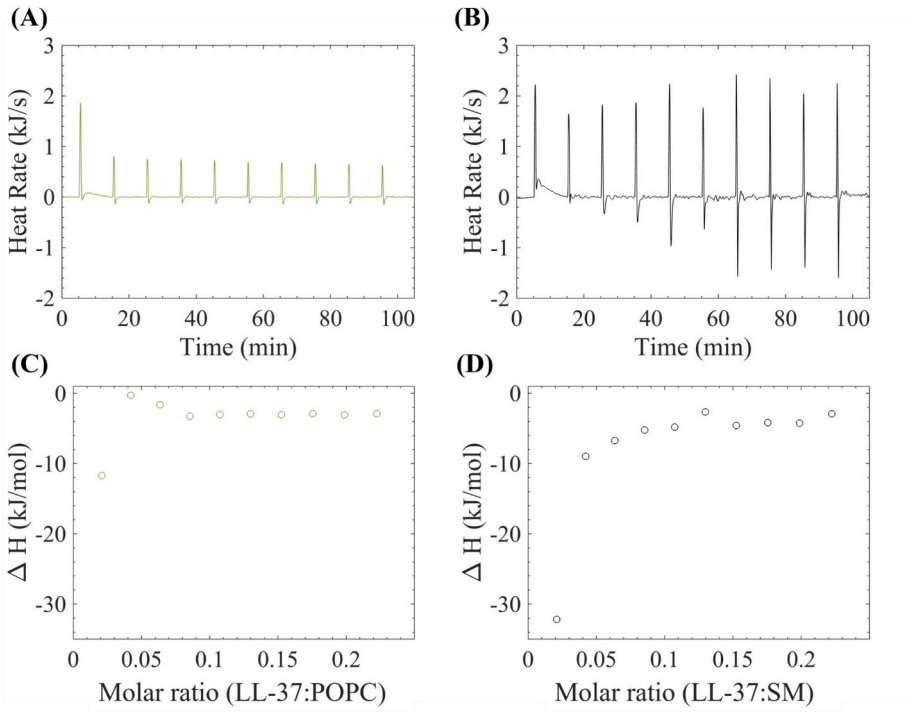

Fig. 4. Representative ITC thermograms of the interaction between LL-37 and **(A)** POPC and **(B)** SM vesicles. **(C)** and **(D)** correspond to the respective enthalpy changes as function of the peptide-to-lipid molar ratio. The experiments were performed at 37 °C in duplicate.

ATR-FTIR setup does not permit measurements at lower temperatures without significant distortions in the data due to ice formation. For this reason, it is not possible to measure the gel to liquid-crystalline phase transition of pure POPC in the absence of CHO since this phase transition occurs below 5 °C.

3.2. *Affinity of lipid-peptide interactions by ITC*

Isothermal titration calorimetry (ITC) is one of the most utilized techniques to obtain information regarding the thermodynamic properties of the interaction between two molecules. This technique is based on the measurement of the heat generated or absorbed due to the interaction during the binding process at constant temperature [35,36].

To characterize the interaction between LL-37 and lipid membranes, ITC was employed. Fig. 4 shows the heat of binding curves as a function of peptide to lipid molar ratio for the individual lipid components POPC, and SM vesicles. By observing the raw heats response, the titration of LL-37 produced homogeneous exothermic peaks with POPC (Fig. 4A), while a combination of exothermic-endothermic patterns with SM system (Fig. 4B). The bindings isotherms, derived from the integration of these

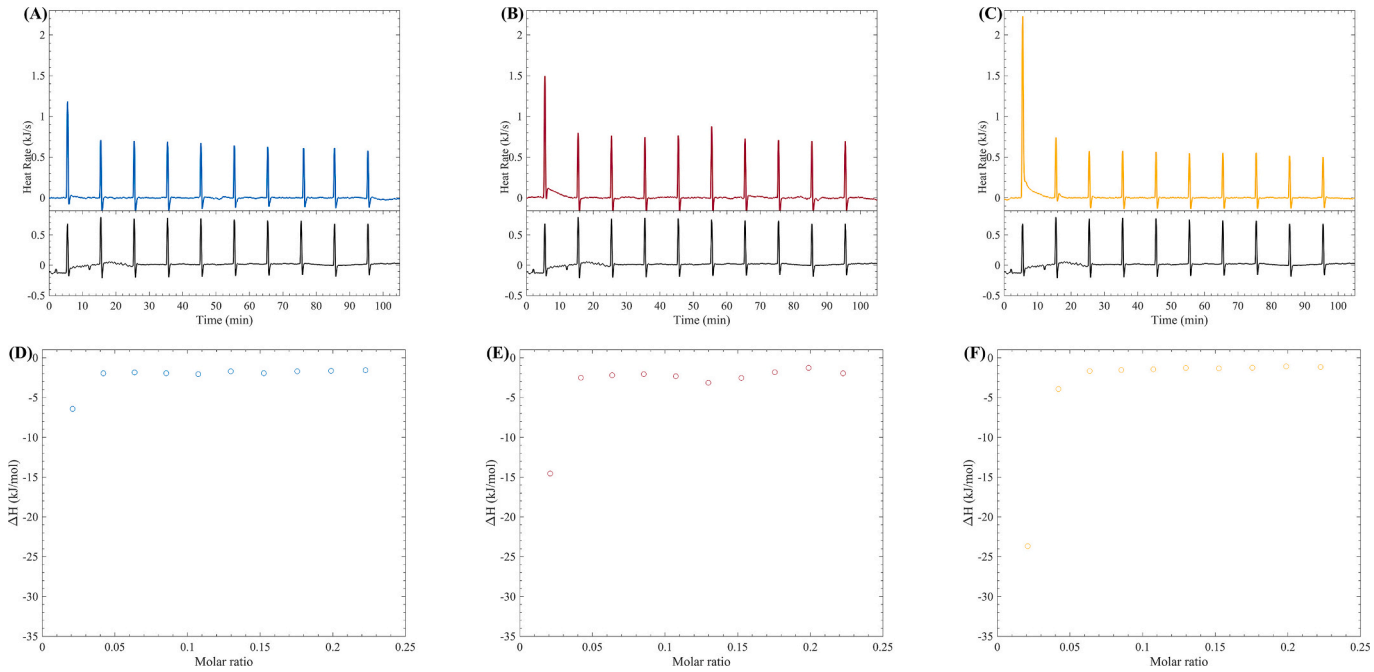

Fig. 5. Representative ITC thermograms of the interaction between LL-37 and **(A)** POPC:SM (50:50 mol%), **(B)** POPC:SM:CHO (45:45:10 mol%), and **(C)** POPC:SM:CHO (40:40:20 mol%) membrane models. While **(D—F)** correspond to the respective enthalpy changes as function of the peptide-to-lipid molar ratio. The experiments were performed at 37 °C in duplicate.

signals, revealed a clear lipid-dependent affinity for AMP where SM showed higher affinity than POPC system. It is important to note that the exothermic signals are primarily attributed to molecular association phenomenon through various interactions, including hydrogen bonding, coulombic forces and van der Waals interactions. However, regardless of the nature of the interaction, exothermic peaks may indicate peptide association with the membrane surface in a concentration-dependent manner. It can be observed that negative ΔH values reflect a significant association between LL-37 peptide and the lipid membrane. Nevertheless, SM not only exhibits a slightly higher interaction but also demonstrates a gradual increase in endothermic peaks, which can be linked to membrane destabilization due to peptide accumulation.

To further investigate a more robust membrane model and examine how CHO modulates these interactions, Fig. 5 presents the ITC thermograms for LL-37 and ternary lipid systems. The raw thermograms systematically sampled only the appearance of initial exothermic peaks that progressively increased with larger CHO content (Figs. 5A–C). The binding isotherm for LL-37 into POPC:SM (50:50 mol%) vesicles showed an initial enthalpy of $\Delta H = -6.5$ kJ mol^{-1} (see Fig. 5D), reflecting similar homogeneous behavior as depicted by POPC (see Fig. 4A). Notably, upon the addition of 10 mol% CHO, the binding became enthalpically more favorable ($\Delta H = -14.7$ kJ mol^{-1}), more than doubling of the binary system (Fig. 5E). This trend was further amplified in the presence of 20 mol% CHO, yielding an initial $\Delta H = -23.8$ kJ mol^{-1} (Fig. 5F), which might indicate a higher affinity of the peptide to the lipid bilayer when CHO is present after adding peptide to the system.

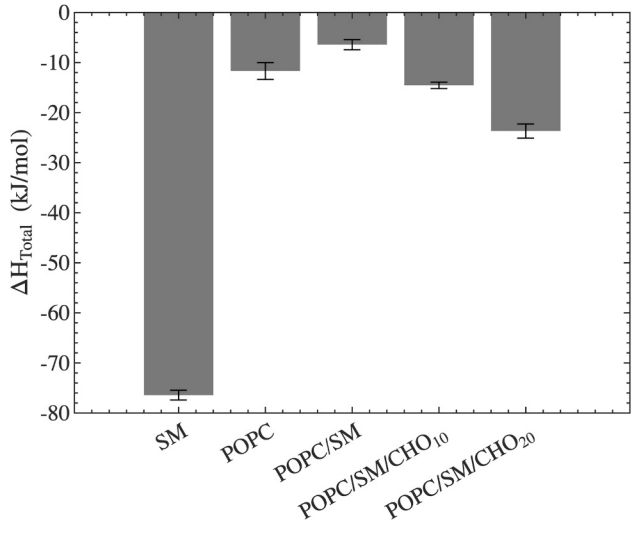

Fig. 6. Total enthalpy change (ΔH_{Total}) of the peptide–lipid interaction as a function of lipid composition. ΔHTotal was calculated as the cumulative heats obtained from the integration of the peaks across the 10 injections depicted in Figs. 4 and 5.

To better illustrate the multi-component influence of lipids in the binding affinities of LL-37, Fig. 6 presents the integration of all ITC peaks across the 10 titrations shown in Figs. 4 and 5, named as total enthalpy change (ΔH_{Total}). These results clearly demonstrated an interesting lipid composition dependence of the ΔH_{Total} values. All together, these results highlight the role of CHO as a linker in the peptide-membrane interaction. This can be interpreted as either a peptide association with the membrane surface or peptide anchoring/partitioning within the lipid bilayer. However, to further inquire how AMP influences the final stabilization or destabilization state of lipid membranes, we next performed DSC analysis.

3.3. Thermotropic behavior by DSC

DSC technique has been widely applied in combination with infrared spectroscopy to study the thermotropic phase behavior of lipid membrane models and the effects associated with drug-membrane interactions [37,38]. To evaluate the influence of LL-37 peptide on the thermotropic phase behavior of the lipid membrane models, samples were analyzed by DSC right after the peptide ITC experiments. Fig. 7 illustrates the thermograms for individual lipid components POPC and SM. Fig. 7a shows the characteristic main gel to liquid-crystalline phase transition of POPC centered around −5.59 °C and presenting a change in enthalpy of $\Delta H = 18.5$ kJ mol^{-1}. This result is in accordance with

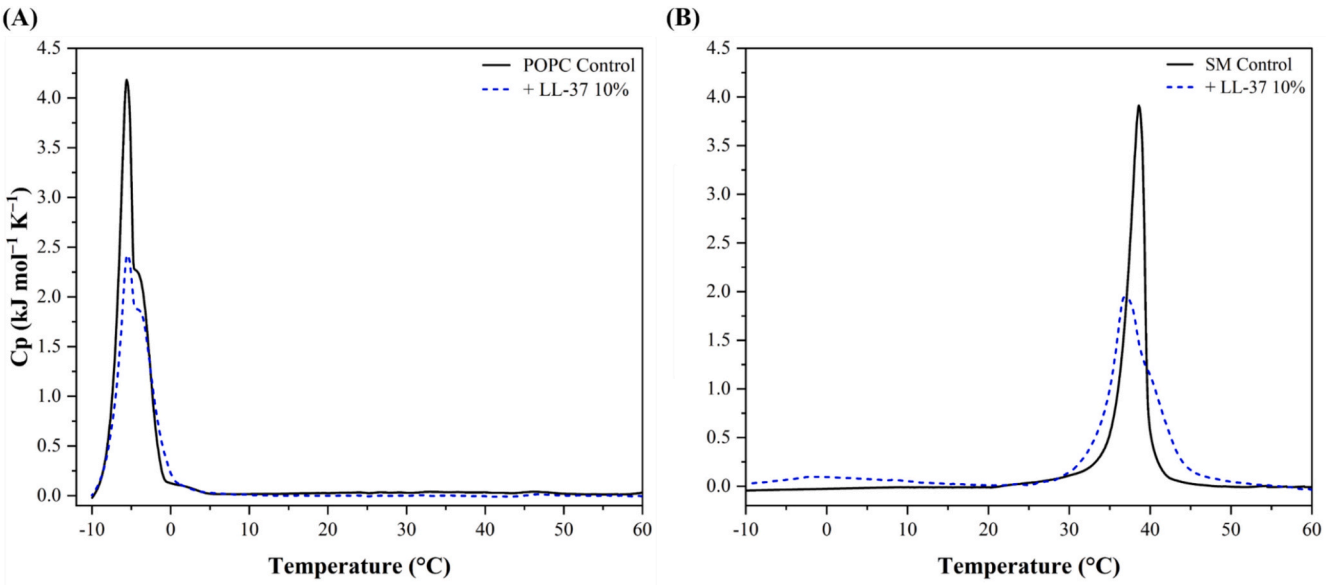

Fig. 7. Representative DSC thermograms of individual lipid species after AMP ITC experimenst. MLVs (1 mM) of **(A)** POPC and **(B)** SM in the absence and presence of LL-37 (10 mol%). Experiments were conducted under the same conditions as in the previous section and represent three independent experiments.

Table 2
Main phase transition temperatures (T_m), global enthalpy (ΔH) and entropy (ΔS) changes from DSC thermograms of pure POPC, and SM vesicles including mixture with LL-37 at 10 mol%. The main phase transition temperature and enthalpy accuracy were ± 0.01 °C and ± 0.8 kJ mol^{-1}, respectively.

Lipid System	Thermodynamics Parameters		
	T_m (°C)	ΔH (kJ mol^{-1})	ΔS (kJ mol^{-1} K^{-1})
POPC	−5.59	18.5	0.07
POPC + LL-37	−5.53	10.8	0.04
SM	38.71	24.2	0.05
SM + LL-37	36.86	13.3	0.04

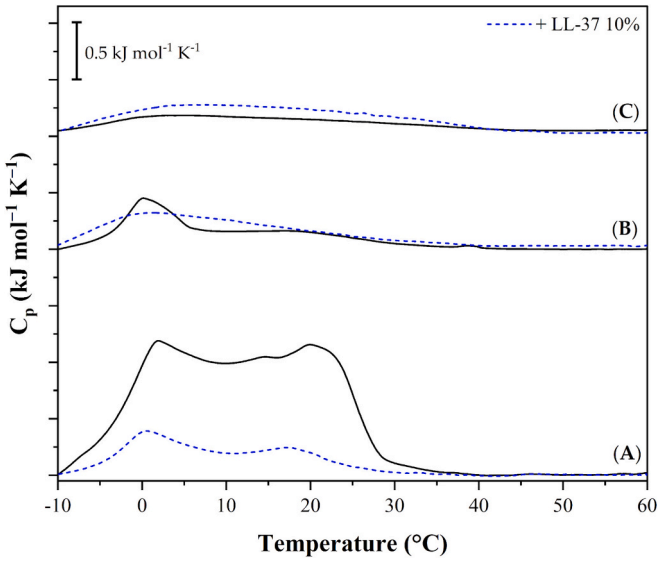

Fig. 8. Representative DSC thermograms of eukaryotic membrane models after AMP kinetics. MLVs (1 mM) of **(A)** POPC:SM (50:50), **(B)** POPC:SM:CHO (45:45:10), and **(C)** POPC:SM:CHO (40:40:20) in the absence and presence of LL-37 (10 mol%, –-- dashed lines). Experiments were conducted under the same conditions as in the previous section and represent three independent experiments.

previous literature reports [39–41]. The interaction of LL-37 with POPC vesicles altered the cooperativity of the chain-melting event, significantly reducing the peak height and enthalpy, down to ΔH = 10.8 kJ mol^{-1} without showing significant changes in T_m (~0.1 °C).

The thermogram record of pure SM vesicles, the second most abundant lipid in the model system, is presented in Fig. 7B. Its calorimetric record shows an endothermic event characterized by a single sharp peak at 38.71 °C with a change in enthalpy of ΔH = 24.2 kJ mol^{-1}, consistent with previous literature reports [42–44]. Interaction of LL-37 with SM vesicles remarkably reduces the height of the peak and alters the cooperativity of the SM transition with a change in enthalpy value (ΔH = 10.9 kJ mol^{-1}). However, the T_m of transition was only slightly affected according to the DSC thermogram, only a mild shift of ~1.8 °C was observed. The thermodynamics parameters associated with the change of phase from lamellar gel phase (L_β) to the lamellar liquid-crystalline (L_α), also known as L-disordered (L_d) phase, including the main transition temperature (T_m), and the change in enthalpy (ΔH), the amount of energy involved in the calorimetric event, are summarized in Table 2.

The thermotropic behavior of the multi-component systems are shown in Fig. 8. The binary lipid mixture POPC:SM (50:50 mol%)

Table 3
Main phase transition temperatures (Tm), global enthalpy (ΔH) and entropy (ΔS) changes from DSC thermograms of mixture systems POPC:SM (50:50 mol %) vesicles with 10–20 mol% CHO addition, including mixture with LL-37 at 10 mol%. The main phase transition temperature and enthalpy accuracy were ± 0.01 °C and ± 0.8 kJ mol^{-1}, respectively.

Lipid System	Thermodynamics Parameters				
	$T_{,1}$ (°C)	$T_{,2}$ (°C)	$T_{,3}$ (°C)	ΔH (kJ mol^{-1})	ΔS (kJ mol^{-1} K^{-1})
POPC:SM	1.96	14.73	19.86	26.5	0.09
POPC:SM + LL-37	0.95	18.46	–	7.0	0.03
POPC:SM:CHO 10%	0.20	17.99	38.66	7.1	0.03
POPC:SM:CHO 10% + LL-37	1.13	–	–	7.2	0.03
POPC:SM:CHO 20%	–	–	–	4.2	0.01
POPC:SM:CHO 20% + LL-37	–	–	–	6.7	0.02

– means not determined.

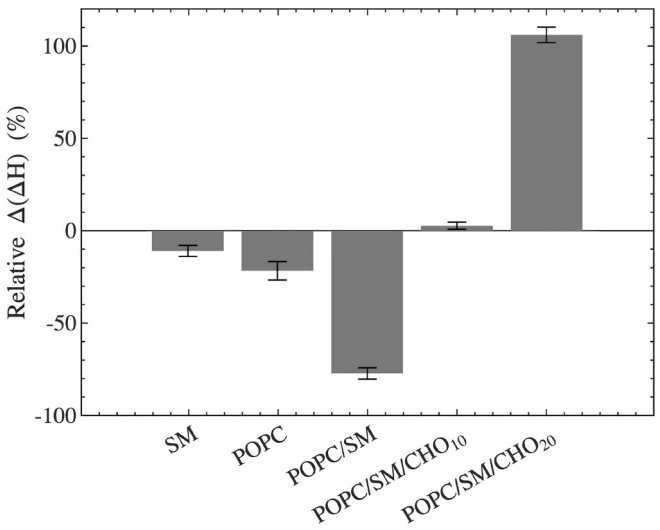

Fig. 9. Relative change in the enthalpy of the global lipid phase transition with and without LL-37 for determined lipid systems, where $\Delta(\Delta H) = \Delta H_{+LL37} - \Delta H_{-LL37}$. Individual ΔH values were taken from Tables 2 and 3.

exhibits a complex profile with at least three endothermic peaks under the envelope (see Fig. 8A). This complexity may be associated with an heterogeneous lipid distribution, or non-ideal mixing, due to the hydrocarbon chain diversity between these two lipid components [29]. It is important to emphasize that thermodynamic theory permits only two coexisting phases in a two-component system. However, although Egg SM extract primarily contains an 86% of 16:0 for the average fatty acid distribution, as indicated by the manufacturer, other lipid species present could be responsible for the observed multipeak response at 14.73 °C.

It is well-known that adding CHO leads to the formation of a third phase in this type of ternary mixtures, known as the liquid-ordered (L_o) phase, in addition to L_β and L_d phases [45–47]. Due to the specific composition used in this study such phase separation is expected to occur in a broad temperature regime [29]. Indeed, when incorporating 10 mol% CHO, our DSC results illustrate a broader thermogram, reflecting the transition between L_o to L_d phase (see Fig. 8B). Additionally, it is also observed that CHO significantly reduces the ΔH of the cooperative melting event (C_p), indicating the formation of the L_o phase [48–50]. The presence of LL-37 significantly alters the shape of the thermogram, broadening the phase transition within the same temperature range, suggesting that AMP promotes mixing when CHO is present.

On the other hand, the addition of 20 mol% CHO to the membrane model resulted in an even larger broadening of the endothermic peak and an overall reduction in the ΔH (see Fig. 8C). Interestingly, when treated with LL-37, membranes require higher ΔH for the melting event, suggesting that AMP not only promotes lipid miscibility as in Fig. 8b, but also leads to an increase in membrane cohesion (ΔH) when CHO is present at this concentration. Table 3 summarizes the thermodynamic parameters of various binary and ternary lipid mixtures, both with and without the interaction of LL-37.

To compare in a more quantitative way the impact of LL-37 on the thermotropic behavior of the various lipid membrane models, global ΔH values from Tables 2 and 3 were utilized. Fig. 9 depicts the relative change in calorimetric enthalpy, Δ(ΔH), upon addition of 10 mol% peptide to five membrane models. Δ(ΔH) is defined as $\Delta H_{+LL37} - \Delta H_{-LL37}$. Thus, negative values of Δ(ΔH) indicate an overall reduction of transition enthalpy or membrane cohesion after AMP treatment, whereas positive values designate an increase. Surprisingly, it is observed that the POPC:SM system undergoes a reduction in the energy required for this melting event by approximately 75%, indicating that peptide was particularly effective at disrupting the membrane cohesion and lipid packing. By contrast, incorporation of 10 mol% cholesterol into the POPC:SM model almost completely suppressed the destabilizing effect of LL-37, restoring Δ(ΔH) to within approximately 5% of the control values. This finding indicates that cholesterol, by enhancing lipid packing in the liquid phase and promoting the formation of a liquid-ordered (L_o) phase, markedly reduces the membrane-disruptive capacity of LL-37.

Remarkably, when 20 mol% CHO was present in the mixture, the enthalpy increases by a factor of 59.5% with addition of LL-37 indicating that the AMP augmented thermal cooperativity, and therefore membrane cohesion, rather than disrupting it. This likely reflects preferential interaction of LL-37 with larger CHO-rich domains (L_o phase). In contrast, vesicles composed of pure POPC and SM displayed moderate negative shifts (~ −20 and − 10%, respectively) in the presence of LL-37, which corresponds to a reduction of the acyl chain order and lower packing density.

The combined calorimetric results suggest that LL-37 exhibits stronger binding affinity and specifically enhances membrane cohesion in CHO-rich domains in a concentration-dependent manner, but only

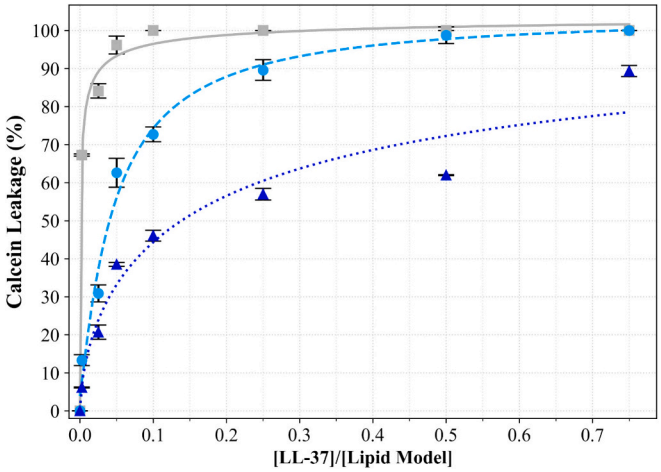

Fig. 10. Percentage of dye leakage as a function of the peptide to lipid molar ratio (P/L) for LL-37 on calcein-LUVs containing POPC:SM (50:50 mol%, ■, solid line), POPC:SM:CHO (45:45:10 mol%, ●, dashed line), and POPC:SM:CHO (45:45:20 mol%, ▲, dotted line) vesicles in HEPES buffer. All measurements were performed at 37 °C. The results represent three independent experiments.

successfully destabilizes cholesterol-poor ones. This may be responsible for the protective effect of CHO against antimicrobial peptide activity. This is supported by an increase in the cooperativity of the phase transitions measured by FT-IR in the presence of 1 mol% LL-37 for the systems that contain CHO (Fig. 1B-C). In summary, while ITC results help us to understand the peptide interaction with the lipid membrane surface, DSC allows us to explore the final thermal-structural state of the membrane once the peptide interplay is established.

3.4. LL-37–induced vesicle leakage as measured by fluorescence spectroscopy

In order to evaluate how lipid composition modulates the membranolytic activity of the LL-37 peptide, calcein release assays were performed. The results of the three lipid systems evaluated with different concentrations of AMP are presented in Fig. 10. In the absence of peptide, no leakage of fluorescent dye from LUVs was observed indicating vesicles stability. Analysis of the LL-37-induced calcein leakage reveals a marked dependence on the lipid composition of the membrane; the inclusion of CHO in the POPC:SM membrane model severely limits the membranolytic activity. For POPC:SM 0.001 P/L molar ratio (or slightly less than 0.1 μM LL-37) was required for 50% leakage, whereas models containing 10 and 20 mol% CHO required ~47-fold (~1.7 μM) and ~ 188-fold (~6.4 μM) higher P/L ratios, respectively, to achieve the same leakage percentage. This substantial loss of activity directly demonstrates that CHO significantly attenuates the LL-37's membranolytic activity.

This ~188-fold increase in the required P/L ratio could confirm the role of CHO as potent structural modulator, rigidifying the bilayer and significantly raising the energetic barrier to AMP insertion and membrane destabilization [19,51]. These results are consistent with the structural data observed in FT-IR and DSC experiments, indicating that the LL-37 acts preferentially on CHO-lacking membranes, which showed that membrane ordering induced by this lipid inhibits the peptide's permeabilization mechanism. Furthermore, the non-linear, concentration-dependent effect presented in all cases confirms the ability of the peptide to induce vesicle breakdown, as reported previously [52,53]. The evident difference in LL-37 concentration required in the CHO presence points directly to the decisive importance of the membrane's physical properties. CHO is well-known for increasing the packing order, mechanical rigidity, and reducing superficial density charge of lipid bilayers while reducing their fluidity.

In summary, with these findings we suggest that the LL-37's membranolytic activity is instead governed by the biophysical properties of the target membrane. Moreover, its potent effect on CHO-lacking membranes, which are characteristic of bacterial or certain viral envelope membranes, underscores its potential as a selective antimicrobial or antiviral agent.

4. Discussion

Since the principal mode of interaction of antimicrobial peptides occurs mainly by disrupting the lipid bilayer membrane of microorganisms, the process involves direct interaction with lipids present in the plasma membrane. The interaction and disruption of the lipid bilayer have been described as occurring in two key steps. First, the AMPs present a differential affinity toward different lipid bilayer surfaces, usually, but not always, driven by electrostatic interactions. The proportion of bound AMPs depends on the concentration of peptide in solution and the affinity constant with the membrane. Secondly, after reaching a threshold concentration, a fraction of the membrane bound AMPs will assume an inserted conformation. The inserted peptides located in the core of the bilayer cause membrane disruption, usually associated with pore formation [54,55]. With the above in mind, it is of biological importance to understand how these two processes can be affected by the presence of different lipid components. Lipids that affect surface charge are likely to influence the binding affinity, and lipids that modify mechanical properties of the membrane will influence the insertion of the peptides. The CHO content of eukaryotic cells has been shown to be a modulator of membrane mechanical properties. Since cholesterol is absent in pathogenic unicellular microorganisms it is therefore relevant to understand if the lytic activity of AMPs is modulated by CHO. However, since membrane mechanical properties may also affect binding affinities by modulating headgroup packing, the capacity of CHO to modulate binding should also be explored. This will help determine if CHO acts as a protective factor that increases the differential activity of AMPs toward microorganisms. The present work contributes to studying the effect that cholesterol has on the activity of the antimicrobial peptide LL-37 and how its content in membrane models can affect the peptide–membrane interactions through biophysical techniques.

In our eukaryotic model systems, CHO was mixed with two of the most abundant components in the plasma membrane of eukaryotic cells [18]; POPC as a monounsaturated phospholipid 16:0–18:1, and egg sphingomyelin (SM) as a naturally occurring sphingolipid containing a heterogeneous fatty acid distribution, 16:0 (86%), 18:0 (6%), 22:0 (3%), 24:1 (3%) and unknown (2%) of the sample [34,42]. Our combined FT-IR spectroscopy, DSC, ITC, and fluorescence data demonstrate that the interaction of the human cathelicidin LL-37 with zwitterionic lipid membranes is strongly modulated by the presence of CHO, with clear consequences on the capacity of LL-37 to disrupt bilayer order, thermotropic lipid behavior, and binding energetic cost. Downward shifts in the phase transition temperature obtained through $\upsilon_s CH_2$ band tracking showed that LL-37 modifies lipid packing by increasing the fluidity of the bilayer across all systems in a concentration dependent manner. This FTIR-ATR data indicates that LL-37 reduces acyl chain order in POPC:SM membranes, yet this effect is meaningfully attenuated by the presence of 10–20 mol% CHO. These findings are consistent with the established role of CHO in condensing lipid bilayers and reducing free-volume defects that favor peptide penetration [21,56]. DSC results improve our understanding of these membrane models because they provide a more detailed analysis of the miscibility of the lipid components and the energetics involved in the melting event. For the proportions of the mixtures used in this work, multiple studies have found that these mixtures present temperature regimes of immiscibility which led to lipid domain formation involving the coexistence of L_o and L_d phases highlighting the importance of this type of mixtures when mimicking the eukaryotic plasma membrane [47,57,58]. The addition of 10 mol% LL-37 lowers peak heat capacity and broadens transitions, signifying diminished enthalpy and cooperativity of the main transition. Similar phenomena have been observed with antimicrobial peptides such as indolicidin and tritrpticin [59], and wild-type antimicrobial peptide isolated from the venom of the spider LyeTx I [60], which also lower and broaden DSC measured transition peaks. In this study, MLVs were used in the DSC experiments due to their larger heat capacity compared to LUVs. This technical choice enhances equipment sensitivity and facilitates the detection of thermotropic changes in lipid mixtures with low cooperativity, especially when peptides or drugs can reduce it even further. Although MLVs limit peptide access to inner lipid layers, this restriction is uniform across all experimental conditions and does not compromise the conclusions regarding cholesterol's role in peptide-membrane interactions.

The effect of AMPs on these thermodynamic properties is an indication of disrupted lipid-lipid interactions and diminished cooperativity. This disruption is particularly evident in the DSC data, where the broadening and lowering of transition peaks reflect the peptide's ability to perturb lipid packing and fluidize the bilayer. In POPC:SM and the mixtures containing CHO two points stand out. First, CHO by itself depresses and broadens transitions in the mixtures, reflecting the emergence of heterogeneity and liquid-ordered domain formation. Second, the effect of LL-37 on the phase transition is dampened by the presence of CHO, where 20 mol% CHO reduces drastically the effect of the

peptide on the transition temperature. This implies that the increased packing induced by CHO dampens against peptide-driven membrane disordering. The data point to a mechanism in which LL-37 perturbs lipid packing, reduces cooperative melting, and fluidizes the bilayer; the extent of this perturbation being dampened by cholesterol content. ITC provides an energetic complement to these structural and thermotropic behavior. LL-37 binding to SM is strongly exothermic, whereas interaction with POPC is weakly exothermic, indicating a preference for ordered, SM-rich environments as observed by FT-IR and DSC. These results agree with investigations into gramicidin S, which demonstrate reduced binding affinity and altered thermodynamic profiles in CHO-containing membranes [61,62]. In addition, Qian and Heller demonstrated that the melittin peptide can induce CHO redistribution into lipid bilayers composed of DMPC:CHO, suggesting that peptide binding can structurally reconfigure lipid domains, reinforcing the concept of domain-driven interactions [63]. The addition of CHO reduces the total ΔH in a concentration-dependent manner, consistent with reduced insertion or a shift toward more superficial binding as CHO content increases.

Although the main function of human cathelicidin LL-37 is antimicrobial activity, its ability to interact with eukaryotic membranes seems contradictory. The results obtained by fluorescence spectroscopy for LL-37 suggest that CHO content modulates the peptide's membranolytic activity, consistent with other reports. Shahmiri and colleagues have confirmed through the quartz crystal microbalance (QCM) study that LL-37 can bind with different affinity to zwitterionic membrane (DMPC: CHO) and negatively charged (DMPC:DMPG), thus suggesting that the ordered liquid phase (L_o) formed by the incorporation of CHO, as was observed in this work by DSC, is essential to weaken the association of LL-37 with the membrane and preserve the membrane of host cells from peptide destabilizing effect [64]. Since CHO changes the viscoelastic properties of the the core, representing a change in the mechanism of action of LL-37 although it is widely described that this peptide can promote pore formation in the lipid bilayer [53,65,66]. Our results are related to the work of Zhang et. Al, who found that the addition of 20 mol% CHO counteracts the leakage of calcein in a membrane model composed of POPC:POPG:CHO (eukaryotic membrane), compared to the model POPC:POPG (bacterial membrane) [65]. While LL-37 is not cytotoxic to human eukaryotic cells at concentrations up to 10 μM [66,67], this observation is consistent with our fluorescence data. Specifically, the inclusion of 20 mol% CHO in the model membrane significantly attenuates membrane destabilization, reducing the membranolytic activity of LL-37 by approximately 55% compared to the POPC:SM (50:50 mol%) system. In contrast, LL-37 exhibits bactericidal activity at much lower concentration, being effective below 3 μM against *E. coli* and as low as 0.25 μM against *S. aureus* [65,68]. These findings indicate that the antimicrobial activity of the concentration at which LL-37 occurs at concentrations below those associated with cytotoxic effects in the antimicrobial activity of eukaryotic cells. Additionally, it has been reported that 20–40 μM of LL-37 is required to achieve ~10% human erythrocyte hemolysis [69].

Interestingly other molecules have similar behavior to cholesterol in terms of membrane properties such as ergosterol, lanosterol because they increase acyl chain order, decrease lipid mobility, and reduce the area per lipid, thereby promoting tighter lipid packing and increased bilayer rigidity [70,71]. These effects lead to reduced free volume and enhanced lateral cohesion within the bilayer, which hinders peptide insertion and limit membrane disruption. Consistently, it has been shown that sterols that strongly promote tight lipid packing decrease peptide binding, membrane leakage, and amyloid formation, highlighting the central role of membrane order in regulating membrane-peptide interactions [72]. Moreover, increased cholesterol levels have been associated with reduced membrane fluidity and decreased susceptibility to peptide-induced permeabilization, despite modulating peptide clustering at the membrane interface [73].

In this sense, recently has been reported that Coenzyme Q10 (CoQ10) a lipophilic isoprenoid residing mainly within the cell in the inner membrane of mitochondrial present is minimal lipid content ratio of lipid membrane (0.5-2 mol%) would influence membrane structure and behavior [74]. Therefore, cholesterol and CoQ10 might have similar protective role against membrane active peptides due to both changing the physicochemical properties of lipid membrane.

As to AMP such as LL-37, this peptide shares important mechanics with amyloidogenic peptides, including their ability to bind, insert to, and disrupt lipid membrane through perturbation of lipid packing and induction of membrane permeabilization. In this context, membrane physicochemical properties play a central role in modulating peptide activity. Recent studies have shown that increasing membrane packing within the hydrophobic core, for example, through incorporation of CoQ10 enhances membrane mechanical stability and significantly reduces both fibrillization and membrane permeabilization induced by amyloidogenic peptides such as Aβ and IAPP [74].

In agreement with this framework, our results indicate that cholesterol attenuates LL-37 membrane interaction, likely by enhancing lipid packing and reducing bilayer susceptibility to disruption. These findings support the concept that modulation of membrane order and rigidity represents a general mechanism governing the activity of both antimicrobial and amyloidogenic peptides.In general, CHO decreases the driving force of the structural lipid work needed to accommodate LL-37. Our results demonstrate that antimicrobial peptide interacts with lipid bilayers in a non-selective way, but the mode and magnitude of perturbation strongly depend on membrane order and CHO content. In low-order or heterogeneous membranes, LL-37 acts predominantly as a disordering and destabilizing agent, while in high-CHO systems, its interaction leads to membrane stabilization or ordering. This non-selective interaction profile underscores the importance of lipid composition in modulating peptide function and suggests that peptide association alone does not predict membrane disruption. The perturbation of lipid bilayers by LL-37 is strongly modulated by membrane composition, with the highest destabilizing effect observed in mixed POPC:SM membranes lacking CHO, and a dramatic shift toward enthalpy rising in highly CHO-enriched systems.

We notice that cholesterol counteracts these effects by stiffening and ordering the membrane, reducing the extent of insertion and the associated rearrangements. At 10 mol% CHO, the bilayer still presents accessible ordered SM-enriched regions that LL-37 can destabilize, whereas at 20 mol% CHO induced reduction of free-volume and defect density likely limits but does not completely inhibit interaction or depth penetration. The findings found in this work are in line with some biological contexts, McGee and colleagues observed that *Helicobacter pylori* steal host CHO, this process attenuated antibacterial efficacy of LL-37 peptide [75]. The authors underscore the cell-surface protective role of CHO and the ability of some microorganisms to incorporate it into their cell membrane as a defense mechanism against antibiotics or AMPs [76]. In contrast, Kiper et al. recently evaluated several antimicrobial bioactive peptides, including LL-37, against *Plasmodium falciparum* (*Pf*), the causative agent of human malaria. The authors demonstrated that these peptides selectively interact with Pf-infected red blood cells (RBCs) as a consequence of two major membrane alterations induced by the parasite: a reduction in cholesterol content and an increased exposure of negatively charged phosphatidylserine on the RBC membrane. Importantly, their findings highlight that the presence of cholesterol—rather than the absence of PS—is the dominant factor inhibiting the activity of antimicrobial peptides [77]. Additionally, few studies have explored peptide interactions in ternary lipid systems POPC:SM:CHO. One notable investigation found that AMPs induce less disruption in liquid-ordered phase (L_o) above a CHO threshold (~20 mol%) than in liquid-disordered phase ($L_{d.}$), with steep reductions in permeabilization past this barrier [78]. This threshold aligns closely with our observations, where 20 mol% CHO significantly dampened LL-37-induced effects and reinforces the idea that the selectivity of AMPs depends not only on the lipid phase but also on the presence of phase separation in

heterogeneous lipid systems. These case studies reinforce the idea that CHO-rich membranes are less susceptible to peptide binding, consistent with our results.

In summary, this work contributes to existing understanding of modulatory effects of cholesterol on peptide-membrane interactions, offering new insights using domain-forming lipid models, and integrated biophysical techniques. It emphasizes that CHO not only modulates peptide binding but also shifts the structural and energetic landscape of interaction. The findings deepen our understanding of peptide selectivity and membrane-targeted therapeutic design.

5. Conclusions

The present study provides novel insights into the CHO-dependent modulation of LL-37 peptide interactions with lipid membranes, combining structural, thermodynamic, and calorimetric evidence. Results consistently indicate that LL-37 perturbs acyl chain order and destabilizes bilayer transitions in POPC:SM systems, whereas CHO significantly mitigates these effects. The progressive reduction in binding enthalpy and the preservation of cooperative lipid transitions highlight the central role of CHO in stabilizing bilayer structure. Importantly, the use of ternary POPC:SM:CHO mixtures reflect the complexity of eukaryotic membranes, surpassing the limitations of single-component models and allowing a more realistic interpretation of peptide activity. This biophysical study confirms the function of CHO as a modulator of peptide selectivity and reinforces the concept that lipid composition dictates the balance between peptide efficacy and membrane protection. Collectively, the findings establish a framework for future studies exploring bioactive peptides in biologically relevant systems, contributing to the rational design of new selective AMPs with therapeutic potential applications.

CRediT authorship contribution statement

Juan M. Giraldo-Lorza: Writing – original draft, Investigation, Formal analysis. **Saúl Antonio Hernández Martínez:** Methodology, Investigation, Formal analysis. **Francisco J. Sierra-Valdez:** Writing – review & editing, Supervision, Resources, Formal analysis, Conceptualization. **Chad Leidy:** Writing – review & editing, Methodology, Conceptualization. **Elizabeth Suesca:** Methodology, Investigation. **Marcela Manrique-Moreno:** Writing – review & editing, Supervision, Project administration, Funding acquisition, Formal analysis, Conceptualization.

Funding

This research was financially supported by the University of Antioquia (CODI Grant 2024–66871), an internal grant of the Faculty of Sciences at Universidad de los Andes (IN*V*-2025-213-3435), and the financial support for this work by the Federico Baur endowed chair in Nanotechnology (0020206BA1) at Tecnológico de Monterrey.

Declaration of competing interest

The authors declare that they have no known competing financial interests or personal relationships that could have appeared to influence the work reported in this paper.

Acknowledgements

J.M. G.-L. wants to thank the University of Antioquia for the master's scholarship. F.J. S.-V. would like to thank the School of Engineering and Science and the FEMSA-Biotechnology Center at Tecnológico de Monterrey for their support through the Aging & Longevity Research Groups from Tecnológico de Monterrey-Campus Monterrey.

Data availability

Data will be made available on request.

References

[1] E.M. Kościuczuk, P. Lisowski, J. Jarczak, N. Strzałkowska, A. Jóźwik, J. Horbańczuk, J. Krzyżewski, L. Zwierzchowski, E. Bagnicka, Cathelicidins: family of antimicrobial peptides. A review, Mol. Biol. Rep. 39 (2012) 10957–10970.
[2] J. Tokajuk, P. Deptuła, E. Piktel, T. Daniluk, S. Chmielewska, T. Wollny, P. Wolak, K. Fiedoruk, R. Bucki, Cathelicidin LL-37 in health and diseases of the oral cavity, Biomedicines 10 (2022) 1086.
[3] M.A. Alford, B. Baquir, F.L. Santana, E.F. Haney, R.E. Hancock, Cathelicidin host defense peptides and inflammatory signaling: striking a balance, Front. Microbiol. 11 (2020) 1902.
[4] H. Memariani, M. Memariani, Antibiofilm properties of cathelicidin LL-37: an in-depth review, World J. Microbiol. Biotechnol. 39 (2023) 99.
[5] N. Mookherjee, M.A. Anderson, H.P. Haagsman, D.J. Davidson, Antimicrobial host defence peptides: functions and clinical potential, Nat. Rev. Drug Discov. 19 (2020) 311–332.
[6] B. Pahar, S. Madonna, A. Das, C. Albanesi, G. Girolomoni, Immunomodulatory role of the antimicrobial LL-37 peptide in autoimmune diseases and viral infections, Vaccines 8 (2020) 517.
[7] M. Zanetti, R. Gennaro, M. Scocchi, B. Skerlavaj, Structure and Biology of Cathelicidins, 1 ed., Springer, New York, NY, 2002.
[8] B. Yang, D. Good, T. Mosaiab, W. Liu, G. Ni, J. Kaur, X. Liu, C. Jessop, L. Yang, R. Fadhil, Significance of LL-37 on immunomodulation and disease outcome, Biomed. Res. Int. (2020) (2020) 8349712.
[9] K.E. Ridyard, J.J.A. Overhage, The Potential of human peptide LL-37 as an antimicrobial and anti-biofilm agent, 2021, p. 650.
[10] M.F. Burton, P.G. Steel, The chemistry and biology of LL-37, Nat. Prod. Rep. 26 (2009) 1572–1584.
[11] U.H. Dürr, U. Sudheendra, A. Ramamoorthy, LL-37, the only human member of the cathelicidin family of antimicrobial peptides, Biochim. Biophys. Acta - Biomembr. 1758 (2006) 1408–1425.
[12] A. Moreno-Angarita, C.C. Aragón, G.J. Tobón, Cathelicidin LL-37: a new important molecule in the pathophysiology of systemic lupus erythematosus, J. Transl. Autoimmun. 3 (2020) 100029.
[13] L. Tapia, B. Garcia-Fojeda, N. Kronqvist, J. Johansson, C. Casals, The collectin SP-A and its trimeric recombinant fragment protect alveolar epithelial cells from the cytotoxic and proinflammatory effects of human cathelicidin in vitro, Front. Immunol. 13 (2022) 994328.
[14] K.A. Henzler Wildman, D.-K. Lee, A. Ramamoorthy, Mechanism of lipid bilayer disruption by the human antimicrobial peptide, LL-37, Biochemistry (Mosc) 42 (2003) 6545–6558.
[15] W.K. Subczynski, M. Pasenkiewicz-Gierula, J. Widomska, L. Mainali, M. Raguz, High cholesterol/low cholesterol: effects in biological membranes: a review, Cell Biochem. Biophys. 75 (2017) 369–385.
[16] T. Harayama, H. Riezman, Understanding the diversity of membrane lipid composition, Nat. Rev. Mol. Cell Biol. 19 (2018) 281–296.
[17] C.T. Boughter, V. Monje-Galvan, W. Im, J.B. Klauda, Influence of cholesterol on phospholipid bilayer structure and dynamics, J. Phys. Chem. B 120 (2016) 11761–11772.
[18] J.M. Giraldo-Lorza, C. Leidy, M. Manrique-Moreno, The influence of cholesterol on membrane targeted bioactive peptides: modulating peptide activity through changes in bilayer biophysical properties, Membranes 14 (2024).
[19] J. Li, X. Lu, W. Ma, Z. Chen, S. Sun, Q. Wang, B. Yuan, K. Yang, Cholesterols work as a molecular regulator of the antimicrobial peptide-membrane interactions, Front. Mol. Biosci. 8 (2021) 638988.
[20] G.P. Pattnaik, H. Chakraborty, Cholesterol alters the inhibitory efficiency of peptide-based membrane fusion inhibitor, Biochim. Biophys. Acta Biomembr. 1861 (2019) 183056.
[21] S. Das, R. Jain, K.K. Banerjee, P. Maity, K. Chattopadhyay, S. Karmakar, Cholesterol Affects the Pore Formation and the Membrane–Membrane Interaction Induced by an Antimicrobial Peptide, NK-2, in Phospholipid Vesicles, J. Memb. Biol. 258 (2025) 237–252.
[22] G. Carta, E. Murru, S. Banni, C. Manca, Palmitic acid: physiological role, metabolism and nutritional implications, Front. Physiol. 8 (2017) 902.
[23] O. Ali, A. Szabó, Review of eukaryote cellular membrane lipid composition, with special attention to the fatty acids, Int. J. Mol. Sci. 24 (2023) 15693.
[24] B.N.A. Mbadugha, F.M. Menger, Sugar/steroid/sugar conjugates: sensitivity of lipid binding to sugar structure, Org. Lett. 5 (2003) 4041–4044.
[25] R.N. Lewis, R.N. McElhaney, Vibrational Spectroscopy of Lipids, in: Handbook of vibrational spectroscopy, 2002.
[26] R.N. Lewis, R.N. McElhaney, Membrane lipid phase transitions and phase organization studied by Fourier transform infrared spectroscopy, Biochim. Biophys. Acta - Biomembr. 1828 (2013) 2347–2358.
[27] B.Y. van Duyl, D. Ganchev, V. Chupin, B. de Kruijff, J.A. Killian, Sphingomyelin is much more effective than saturated phosphatidylcholine in excluding unsaturated phosphatidylcholine from domains formed with cholesterol, FEBS Lett. 547 (2003) 101–106.
[28] J.P. Slotte, The importance of hydrogen bonding in sphingomyelin's membrane interactions with co-lipids, Biochim. Biophys. Acta Biomembr. 2016 (1858) 304–310.

[29] R.F. De Almeida, A. Fedorov, M. Prieto, Sphingomyelin/phosphatidylcholine/cholesterol phase diagram: boundaries and composition of lipid rafts, Biophys. J. 85 (2003) 2406–2416.
[30] K. Jacobson, P. Liu, B.C. Lagerholm, The lateral organization and mobility of plasma membrane components, Cell 177 (2019) 806–819.
[31] M.C. Klaiss-Luna, M. Manrique-Moreno, Infrared spectroscopic study of multi-component lipid systems: a closer approximation to biological membrane fluidity, Membranes 12 (2022) 534.
[32] Z.Ö. Çetinel, D. Bilge, The effects of miltefosine on the structure and dynamics of DPPC and DPPS liposomes mimicking normal and cancer cell membranes: FTIR and DSC studies, J. Mol. Liq. 356 (2022) 119041.
[33] Z. Arsov, E.J. González-Ramírez, F.M. Goñi, S. Tristram-Nagle, J.F. Nagle, Phase behavior of palmitoyl and egg sphingomyelin, Chem. Phys. Lipids 213 (2018) 102–110.
[34] K.P. Shaw, N.J. Brooks, J.A. Clarke, O. Ces, J.M. Seddon, R.V. Law, Pressure–temperature phase behaviour of natural sphingomyelin extracts, Soft Matter 8 (2012) 1070–1078.
[35] I.D.L. Cavalcanti, F.H.X. Junior, N.S.S. Magalhães, M.C.D.B.L. Nogueira, Isothermal titration calorimetry (ITC) as a promising tool in pharmaceutical nanotechnology, Int. J. Pharm. 641 (2023) 123063.
[36] K. Lin, G. Wu, Isothermal Titration Calorimetry Assays to Measure Binding Affinities In Vitro, in: The Hippo Pathway: Methods Protocols, 2018, pp. 257–272.
[37] C. Demetzos, Differential scanning calorimetry (DSC): a tool to study the thermal behavior of lipid bilayers and liposomal stability, J. Liposome Res. 18 (2008) 159–173.
[38] R.N. Lewis, D.A. Mannock, R.N. McElhaney, Differential Scanning Calorimetry (DSC) for lipids and lipid membranes, in: Wiley Encyclopedia of Chemical Biology, 2008, pp. 1–11.
[39] H. Takahashi, T. Hayakawa, A. Makino, K. Iwamoto, K. Ito, S.B. Sato, T. Kobayashi, Long chain ceramides raise the main phase transition of monounsaturated phospholipids to physiological temperature, Sci. Rep. 12 (2022) 20803.
[40] J.A. Svetlovics, S.A. Wheaten, P.F. Almeida, Phase separation and fluctuations in mixtures of a saturated and an unsaturated phospholipid, Biophys. J. 102 (2012) 2526–2535.
[41] W. Curatolo, B. Sears, L.J. Neuringer, A calorimetry and deuterium NMR study of mixed model membranes of 1-palmitoyl-2-oleylphosphatidylcholine and saturated phosphatidylcholines, Biochimica et Biophysica acta - Biomembranes 817 (1985) 261–270.
[42] M.C. Klaiss-Luna, M. Jemioła-Rzemińska, K. Strzałka, M. Manrique-Moreno, Understanding the biophysical interaction of LTX-315 with tumoral model membranes, Int. J. Mol. Sci. 24 (2023) 581.
[43] M. Kodama, Y. Kawasaki, H. Ohtaka, The main transition enthalpy of the gel-to-liquid crystal phases for a series of asymmetric chain length d-erythro (2S, 3R) sphingomyelins, Thermochim. Acta 532 (2012) 22–27.
[44] M. Ishinaga, Y. Okita, A. Ito, Calorimetric study on a Dipalmitoylphosphatidylcholine-Propylgallate mixture, J. Biochem. 100 (1986) 1663–1668.
[45] A. Pokorny, L.E. Yandek, A.I. Elegbede, A. Hinderliter, P.F. Almeida, Temperature and composition dependence of the interaction of δ-lysin with ternary mixtures of sphingomyelin/cholesterol/POPC, Biophys. J. 91 (2006) 2184–2197.
[46] C.J. Garvey, S.J. Bryant, A. Elbourne, T. Hunt, B. Kent, M. Kreuzer, M. Strobl, R. Steitz, G. Bryant, Phase separation in a ternary DPPC/DOPC/POPC system with reducing hydration, J. Colloid Interface Sci. 638 (2023) 719–732.
[47] S.L. Veatch, S.L. Keller, Separation of liquid phases in giant vesicles of ternary mixtures of phospholipids and cholesterol, Biophys. J. 85 (2003) 3074–3083.
[48] W.K. Subczynski, M. Pasenkiewicz-Gierula, J. Widomska, N. Stein, Role of cholesterol in maintaining the physical properties of the plasma membrane, Cholesterol (2022) 41–71.
[49] A. Barba-Bon, M. Nilam, A. Hennig, Supramolecular chemistry in the biomembrane, ChemBioChem 21 (2020) 886–910.
[50] I.Y. Hasan, A. Mechler, Analytical approaches to study domain formation in biomimetic membranes, Analyst 142 (2017) 3062–3078.
[51] V.S. Khodade, M. Sharath Chandra, A. Banerjee, S. Lahiri, M. Pulipeta, R. Rangarajan, H. Chakrapani, Bioreductively activated reactive oxygen species (ROS) generators as MRSA inhibitors, ACS Med. Chem. Lett. 5 (2014) 777–781.
[52] K.A. Brogden, Antimicrobial peptides: pore formers or metabolic inhibitors in bacteria? Nat. Rev. Microbiol. 3 (2005) 238–250.
[53] C.-C. Lee, Y. Sun, S. Qian, H.W. Huang, Transmembrane pores formed by human antimicrobial peptide LL-37, Biophys. J. 100 (2011) 1688–1696.
[54] K. Ajesh, K. Sreejith, Antimicrobial Peptides: Challenges and Future Perspectives, Elsevier Science, 2022.
[55] H. Zhang, J. Lv, Z. Ma, J. Ma, J. Chen, Advances in antimicrobial peptides: mechanisms, design innovations, and biomedical potential, Molecules 30 (2025) 1529.
[56] F.T. Doole, T. Kumarage, R. Ashkar, M.F. Brown, Cholesterol stiffening of lipid membranes, J. Memb.Biol. 255 (2022) 385–405.
[57] S.L. Veatch, S.L. Keller, Seeing spots: complex phase behavior in simple membranes, Biochim. Biophys. Acta 1746 (2005) 172–185.
[58] A. Kusumi, T.K. Fujiwara, T.A. Tsunoyama, R.S. Kasai, A.A. Liu, K.M. Hirosawa, M. Kinoshita, N. Matsumori, N. Komura, H. Ando, Defining raft domains in the plasma membrane, Traffic 21 (2020) 106–137.
[59] V.V. Andrushchenko, H.J. Vogel, E.J. Prenner, Interactions of tryptophan-rich cathelicidin antimicrobial peptides with model membranes studied by differential scanning calorimetry, Biochim. Biophys. Acta 1768 (2007) 2447–2458.
[60] A.N. de Souza, G.d.A. Cardoso, L.O. Nunes, C. Aisenbrey, E. Salnikov, K.R. de Souza, A. Saad, M.E. de Lima, J.M. Resende, B. Bechinger, Comparative structural and biophysical investigation of *Lycosa erythrognatha* toxin I (lyeTx I) and its analog LyeTx Ib, Antibiotics 14 (2025) 66.
[61] T. Abraham, R.N. Lewis, R.S. Hodges, R.N. McElhaney, Isothermal titration calorimetry studies of the binding of the antimicrobial peptide gramicidin S to phospholipid bilayer membranes, Biochemistry (Mosc) 44 (2005) 11279–11285.
[62] E.J. Prenner, R.N. Lewis, M. Jelokhani-Niaraki, R.S. Hodges, R.N. McElhaney, Cholesterol attenuates the interaction of the antimicrobial peptide gramicidin S with phospholipid bilayer membranes, Biochim. Biophys. Acta 1510 (2001) 83–92.
[63] S. Qian, W.T. Heller, Melittin-induced cholesterol reorganization in lipid bilayer membranes, Biochim. Biophys. Acta Biomembr. 2015 (1848) 2253–2260.
[64] M. Shahmiri, M. Enciso, C.G. Adda, B.J. Smith, M.A. Perugini, A. Mechler, Membrane core-specific antimicrobial action of cathelicidin LL-37 peptide switches between pore and nanofibre formation, Sci. Rep. 6 (2016) 38184.
[65] X. Zhang, K. Oglęcka, S. Sandgren, M. Belting, E.K. Esbjörner, B. Nordén, A. Gräslund, Dual functions of the human antimicrobial peptide LL-37—target membrane perturbation and host cell cargo delivery, Biomembranes 1798 (2010) 2201–2208.
[66] S. Bhattacharjya, Z. Zhang, A. Ramamoorthy, LL-37: structures, antimicrobial activity, and influence on amyloid-related diseases, Biomolecules 14 (2024) 320.
[67] D. Svensson, B.-O. Nilsson, Human antimicrobial/host defense peptide LL-37 may prevent the spread of a local infection through multiple mechanisms: an update, Inflamm. Res. 74 (2025) 36.
[68] S.N. Dean, B.M. Bishop, M.L. van Hoek, Natural and synthetic cathelicidin peptides with anti-microbial and anti-biofilm activity against Staphylococcus aureus, BMC Microbiol. 11 (2011) 114.
[69] S. Al-Adwani, C. Wallin, M.D. Balhuizen, E.J. Veldhuizen, M. Coorens, M. Landreh, Á. Végvári, M.E. Smith, I. Qvarfordt, A.J.S.r. Lindén, Studies on Citrullinated LL-37: Detection in Human Airways, Antibacterial Effects and Biophysical Properties 10, 2020, p. 2376.
[70] M. Christensen, N.A. Berglund, B. Schiøtt, The effect of cholesterol on membrane-bound islet amyloid polypeptide, Front. Mol. Biosci. 8 (2021).
[71] Z. Cournia, G.M. Ullmann, J.C. Smith, Differential effects of cholesterol, ergosterol and lanosterol on a dipalmitoyl phosphatidylcholine membrane: a molecular dynamics simulation study, J. Phys. Chem. B 111 (2007) 1786–1801.
[72] X. Zhang, E. London, D.P. Raleigh, Sterol Structure Strongly Modulates Membrane–Islet Amyloid Polypeptide Interactions, Biochemistry (Mosc) 57 (2018) 1868–1879.
[73] E.J. Fernández-Pérez, F.J. Sepúlveda, C. Peters, D. Bascuñán, N.O. Riffo-Lepe, J. González-Sanmiguel, S.A. Sánchez, R.W. Peoples, B. Vicente, L.G. Aguayo, Effect of cholesterol on membrane fluidity and association of aβ oligomers and subsequent neuronal damage: a double-edged sword, Front. Aging Neurosci. 10 (2018) 226.
[74] R.M. Seychell, A. El Saghir, G. Farrugia, N. Vassallo, Coenzyme Q10 enhances resilience of mitochondrial-like membranes against amyloidogenic peptides, Membranes 15 (2025) 148.
[75] D.J. McGee, A.E. George, E.A. Trainor, K.E. Horton, E. Hildebrandt, T. L. Testerman, Cholesterol enhances helicobacter pylori resistance to antibiotics and LL-37, Antimicrob. Agents Chemother. 55 (2011) 2897–2904.
[76] Y. Luo, D.T. McLean, G.J. Linden, D.F. McAuley, R. McMullan, F.T. Lundy, The naturally occurring host defense peptide, LL-37, and its truncated mimetics KE-18 and KR-12 have selected biocidal and antibiofilm activities against *Candida albicans*, *Staphylococcus aureus*, and *Escherichia coli* in vitro, Front. Microbiol. 8 (2017) 544.
[77] E. Kiper, D.B. Hur, D. Alfandari, A.C. Camacho, N.A. Wani, G.D. Efrat, M. I. Morandi, M. Goldsmith, R. Rotkopf, R. Kamyshinsky, Antimicrobial peptides selectively target malaria parasites by a cholesterol-dependent mechanism, J. Biol. Chem. 301 (2025).
[78] A.J. McHenry, M.F. Sciacca, J.R. Brender, A. Ramamoorthy, Does cholesterol suppress the antimicrobial peptide induced disruption of lipid raft containing membranes? Biochim. Biophys. Acta 1818 (2012) 3019–3024.